

Article

# Discovery of Ancient Volcanoes in the Okhotsk Sea (Russia): New Constraints on the Opening History of the Kurile Back Arc Basin

Reinhard Werner <sup>1,\*</sup>, Boris Baranov <sup>2</sup>, Kaj Hoernle <sup>1,3</sup>, Paul van den Bogaard <sup>1</sup>, Folkmar Hauff <sup>1</sup> and Igor Tararin <sup>4</sup>

<sup>1</sup> GEOMAR Helmholtz Centre for Ocean Research Kiel, Wischhofstr. 1-3, 24148 Kiel, Germany; khoernle@geomar.de (K.H.); pbogaard@mac.com (P.v.d.B.); fhauff@geomar.de (F.H.)

<sup>2</sup> Shirshov Institute of Oceanology, Nakhimovsky Avenue 36, 117851 Moscow, Russia; bbaranov@ocean.ru

<sup>3</sup> Institute of Geosciences, Kiel University, 24118 Kiel, Germany

<sup>4</sup> Far East Geological Institute RAS, 100-letiya Vladivostoka Prospect 159, 690022 Vladivostok, Russia; tararin@fegi.ru

\* Correspondence: rwwerner@geomar.de; Tel.: +49-431-600-1416

Received: 22 September 2020; Accepted: 4 November 2020; Published: 6 November 2020

**Abstract:** Here we present the first radiometric age and geochemical (major and trace element and isotope) data for samples from the Hydrographer Ridge, a back arc volcano of the Kurile Island Arc, and a newly discovered chain of volcanoes (“Sonne Volcanoes”) on the northwestern continental slope of the Kurile Basin on the opposite side of the arc. The <sup>40</sup>Ar/<sup>39</sup>Ar age and geochemical data show that Hydrographer Ridge (3.2–3.3 Ma) and the “Sonne Volcanoes” (25.3–25.9 Ma) have very similar trace element and isotope characteristics to those of the Kurile Island Arc, indicating derivation from a common magma source. We conclude that the age of the “Sonne Volcanoes” marks the time of opening of the Kurile Basin, implying slow back arc spreading rates of 1.3–1.8 cm/y. Combined with published data from the Kurile fore arc, our data suggest that the processes of subduction, Kurile Basin opening and frontal arc extension occurred synchronously and that extension in the rear part and in the frontal part of the Kurile Island Arc must have been triggered by the same mechanism.

**Keywords:** Kurile Basin; island arc; back arc spreading; volcanoes; geochemistry; Ar/Ar-age dating

---

## 1. Introduction

The Kurile Basin in the Okhotsk Sea (northwestern Pacific) is a back arc basin located behind the Kurile Island Arc (Figure 1). Although it is generally accepted that the Kurile Basin was formed by back arc spreading (Savostin et al., 1983; Kimura and Tamaki 1986; Jolivet 1987; Maeda 1990; Gnibidenko et al., 1995; Baranov et al., 2002a [1–6]), some issues related to the spreading process such as the age of the Kurile Basin opening are still under discussion. Direct evidence for the age of the Kurile Basin floor is lacking, because magnetic lineations have not been found inside the basin and the basin crust has not been sampled directly by dredging or drilling. On the basis of heat flow data, basement depth, seismo-stratigraphy and the age of sedimentary and igneous rocks, the basin was postulated to have formed in Early/Late Oligocene to Middle Miocene (32–15 Ma) (Kimura and Tamaki 1985; Kharakhinov 1996; Hayashi 1997; Karp et al., 2006; Terekhov et al., 2008; Emel’yanova and Lelikov 2016 [2,7–11]). Investigations of magmatism and paleomagnetism of adjacent land areas (Hokkaido and Sakhalin Islands) suggest that spreading in the Kurile Basin could have occurred during the Middle Miocene (16–15 Ma) (Maeda 1990 [4]) or from Early to Late Miocene (~23 to 8 Ma) (Takeuchi et al., 1999; Ikeda et al., 2000 [12,13]).

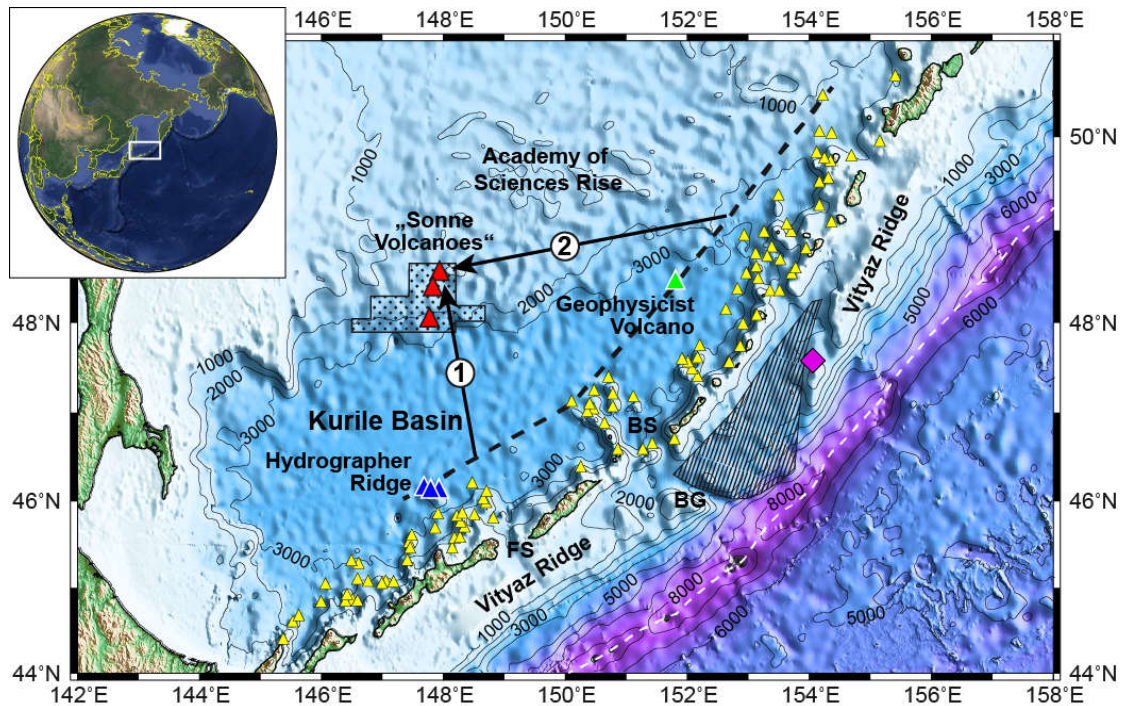


**Figure 1.** Location of the submarine volcanic edifices in the Kurile Island Arc system. Small yellow triangles indicate volcanoes according to Avdeiko et al. (1992) [14]. Large red triangles mark volcanic edifices discovered during the R/V Sonne cruise SO178 and large dark blue (Hydrographer Ridge) and green (Geophysicist volcano) triangles back arc volcanoes which have been investigated in the framework of the German–Russian KOMEX project. Black dashed line connects young or recent back arc volcanoes located at the greatest distance from the trench axis (white dashed line). Black numbered arrows mark the migration track of the “Sonne Volcano” by spreading in (1) SW–NE directions or (2) NNW–SSE direction (2). Arrow #1 roughly corresponds to the axis of the basement rise in the central part of the Kurile Basin. The dotted polygon indicates the area mapped by multi-beam echo-sounding on SO178. The shaded area marks the extent of a recently discovered fore arc extension structure (e.g., Lelikov et al., 2008 [15], Emelyanova et al., 2012 [16]). The purple diamond shows the location of the dredge hauls on the Vityaz Ridge which yielded the trachy-andesite discussed in this study. The base map is from “The GEBCO\_2014 Grid, version 20150318, <http://www.gebco.net>”. Contour interval is 1000 m. BS = Bussol Strait, FS = Frisa Strait, BG = Bussol Graben.

The southeastern margin of the Kurile Basin has a complex structure, because there are many seamounts aligned in the form of an echelon ridges striking into the basin at angles of about 25–90° to the general trend of the Kurile Island Arc (Baranov et al., 2002b [17]). These seamounts are either volcanic chains or faulted arc basement (Gnibidenko et al., 1995 [5]). They occur as discrete volcanic edifices or volcanic ridges, which extend into the Kurile Basin for tens of kilometers, such as a volcanic ridge near the Bussol Straits or Hydrographer Ridge (Baranov et al., 2002b [17]; Figure 1). Dredge samples from the ridge near Bussol Straits have Kurile Island Arc chemical affinities (Avdeiko et al., 1992 [14]). Seismic profiling has revealed that structures morphologically similar to volcanic edifices occur in the abyssal parts of the Kurile Basin (Tuezov 1977 [18]). All of these structures, however, are covered by sediments and are thus inaccessible to direct sampling e.g., by dredging. The only known exception is the submarine Geophysicist volcano investigated during several cruises in the framework of German–Russian project KOMEX (Kurile-Okhotsk Marine Experiment; Nürnberg et al., 1997; Biebow and Hütten 1999 [19,20]). The lavas of Geophysicist Seamount are ~1 My. old and show geochemical signatures very similar to the Kurile Island Arc, indicating that Geophysicist Seamount is a young back arc volcano (Baranov et al., 2002b [17]).

The northwestern margin of the Kurile Basin rises 2300 m above the abyssal plain of the Kurile Basin (Figure 1). Whereas most of the Kurile Basin is underlain by oceanic crust with a thickness of about 10 km (Galperin and Kosminskaya 1964 [21]), seismic refraction data show that its northern margin is underlain by thinned continental crust with a thickness of about 20 km (Galperin and Kosminskaya 1964 [21]). It represents the transition to the oceanic crust of the Kurile Basin. Dredge samples indicate that the northern slope of the Kurile Basin is composed of extrusive, intrusive and metamorphic rocks with geochemical signatures of the calc-alkaline arc series (Baranov et al., 2002b [17]. K–Ar dating revealed that the majority of these rocks are Cretaceous in age (Gribidenko et al., 1995 [5]).

Here we report the results of mapping and sampling of volcanic structures on the slopes of the Kurile Basin. These investigations have been carried out during R/V Akademik Lavrentyev LV29 (2002) (Biebow et al., 2003 [22]) and R/V Sonne SO178 (2004) KOMEX cruises (Dullo et al., 2004 [23]). The LV29 cruise yielded the first in situ samples from the Hydrographer Ridge, an elongated volcanic structure which extends from the southern Kurile back arc into the Kurile Basin (Figures 1 and 2). During SO178, extensive multi-beam mapping of the northwestern slope of the Kurile Basin revealed three to date unknown volcanoes (Figures 1 and 3). These volcanoes, called Sonne Volcanoes by cruise participants, have been sampled by dredging. Mapping, age dating, and geochemical analyses (major and trace elements and Sr-Nd-Pb isotopes) of the rocks recovered from the Hydrographer Ridge and from the Sonne Volcanoes revealed that Hydrographer Ridge is a Late Pliocene back arc volcano, whereas the Sonne Volcanoes represent paleo-Kurile Arc volcanoes, formed in Late Oligocene, and subsequently displaced by extension and seafloor spreading a distance of at least 200 km. Our data also provide new constraints on the opening history of the Kurile Basin and the early history of the Kurile Island Arc.

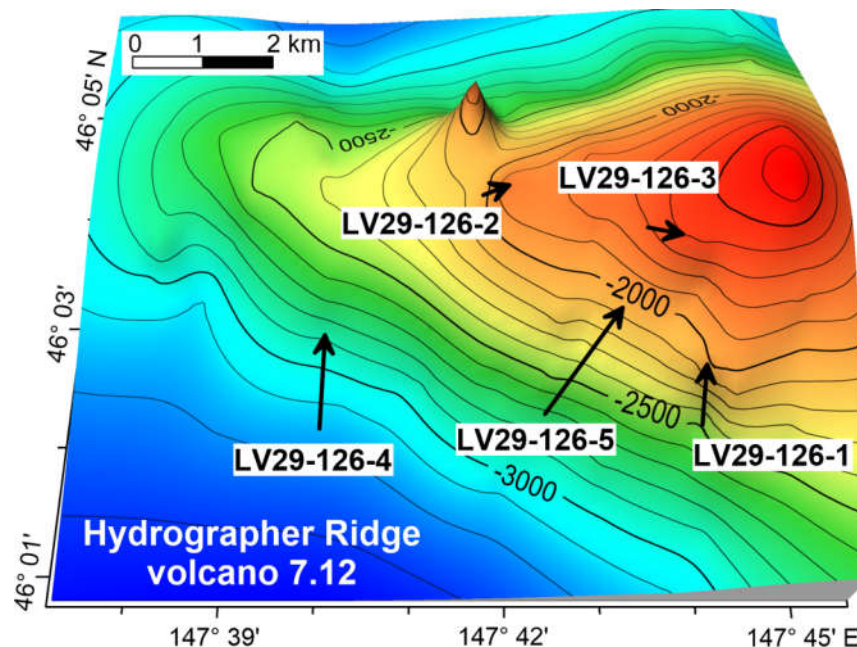


**Figure 2.** Bathymetric map of western Hydrographer Ridge based on single beam echo-sounding data recorded on R/V Akademik Lavrentyev cruise LV29. The arrows show the location of the dredge hauls conducted on cruise LV29. Dredges LV 126-1 and -4 yielded the samples analyzed for this study. The location of the Hydrographer Ridge is shown on Figure 1 as dark blue triangles.

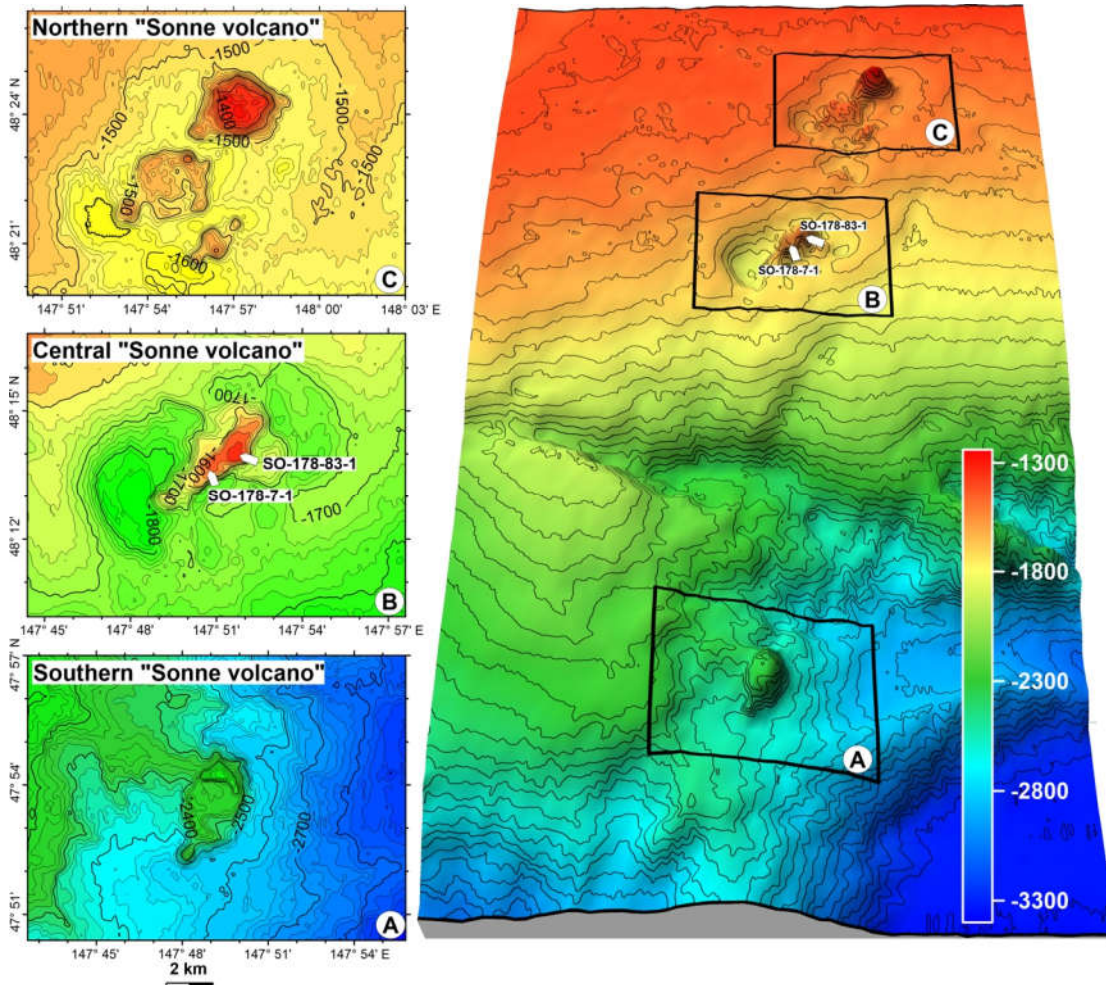


**Figure 3.** Bathymetric map showing the Sonne Volcanoes on the northern slope of the Kurile Basin with insets for the (A) southern, (B) central and (C) northern Sonne Volcanoes. Thick labeled lines indicate dredge hauls which yielded in situ volcanic rocks. Contour interval is 20 m for 2D-maps and 50 m for large 3D map. Locations of the volcanoes are shown on Figure 1 as red triangles.

## 2. Materials and Methods

**Mapping:** The bathymetric survey of the Hydrographer Ridge was carried out during R/V Akademik Lavrentyev LV29 cruise using a ship-mounted narrow beam echo-sounder ELAC LAZ-72 E-V (Wärtsilä ELAC Nautik GmbH, Kiel, Germany) with frequency 12 kHz. The standard accuracy of depth measurement was equal  $\pm 1\%$ . A ship-mounted SIMRAD EM120 multi-beam echo sounder (Kongsberg Maritime AS, Kongsberg, Norway) was used during the bathymetric survey of the Sonne Volcanoes. The EM120 system can map the seafloor with a swath width of up to six times the water depth. The geometric resolution depends on the water depth and the angular coverage sector used. It is less than 10 m at depths of 2000–3000 m. The bathymetric maps (Figures 2 and 3) have been generated using Surfer software.

**Sampling:** Rock sampling on LV29 and SO178 was carried out using chain bag dredges, which are dragged along the ocean floor by the ship's winch. Because ice-rafted material ("dropstones") is common in the Sea of Okhotsk, several criteria were applied to minimize the likelihood of selecting glacial dropstones for analyses. These criteria include angularity of samples, especially those with freshly broken surfaces, because ice-rafted dropstones are typically rounded by glacial transport. Another important criteria is the homogeneity of rock types within a single dredge haul, because dropstones generally form very heterogeneous assemblages.

Ar/Ar-dating: Single-crystal  $^{40}\text{Ar}/^{39}\text{Ar}$  analyses were carried out on amphibole and feldspar phenocrysts. Crystals were handpicked from crushed and sieved splits, cleaned using an ultrasonic disintegrator, and etched in 5% hydrofluoric acid for 15 min. Samples were irradiated at the 5-MW reactor of the Helmholtz Center Geesthacht in aluminum trays and irradiation cans wrapped in cadmium foil. Feldspar and hornblende phenocrysts were sequentially fused in single heating steps. Purified gas samples were analyzed using a MAP 216 series noble gas mass spectrometer. Raw mass spectrometer peaks were corrected for mass discrimination, background, and blank values, determined every fifth analysis. The neutron flux was monitored using Taylor Creek Rhyolite Sanidine (TCR-2:  $27.87 \pm 0.04$  Ma; Lanphere and Dalrymple 2000 [24]). Corrections for interfering neutron reactions on Ca and K are based on analyses of optical grade  $\text{CaF}_2$  and high-purity  $\text{K}_2\text{SO}_4$  salt crystals that were irradiated together with the samples. Internal errors are reported at the 2 sigma confidence level.

Geochemistry: Samples selected for geochemistry were first crushed to small pieces, then washed in deionized water, and carefully hand-picked under a binocular microscope. Major elements and some trace elements (e.g., Cr, Ni, Zr, and Sr) of whole rock samples were determined on fused beads using a Phillips X'Unique PW1480 X-ray fluorescence spectrometer (XRF, Malvern Panalytical B.V., Almelo, Netherlands) equipped with a Rh-tube at GEOMAR.  $\text{H}_2\text{O}$  and  $\text{CO}_2$  were analyzed in an infra-red photometer (Rosemount CSA 5003). Measured and reference values obtained for the JB-2, JB-3, JA-2, and JR-1 standards are shown in Table S1. Additional trace elements (e.g., Rb, Ba, Y, Nb, Ta, Hf, U, Th, Pb, and all REE) for LV29 samples were determined by ICP-MS on a VG Plasmaquad PQ1-ICP-MS at the Institute of Geosciences (University of Kiel) after the methods of Garbe-Schönberg (1993) [25] and for SO178 samples on an ELEMENT 2 at the University of Bremen following the procedures outlined by Schwarz et al. (2005) [26]. Measured values obtained by ICP-MS and reference values for the BCR-2 (Bremen) and BIR-1 (Kiel) standards are shown in Table S2.

Sr-Nd isotope analyses of LV29 samples were carried out on rock powders, leached in 6N HCl at  $130^\circ\text{C}$  for 1 h prior to dissolution in a 5:1 mixture of concentrated ultrapure (u.p.) HF and  $\text{HNO}_3$  u.p. Pb isotope analyses of LV29 samples were conducted on unleached powders and rock chips respectively. Sr-Nd-Pb isotope analyses of SO178 samples were carried out on rock chips, leached in 2N HCl at  $70^\circ\text{C}$  for 30 min prior to dissolution. The element chromatography followed the methods outlined in Hoernle and Tilton (1993) [27]. Sr-Nd-Pb isotopic ratios were determined on the TRITON and MAT262 RPQ2+ thermal ionization mass spectrometers (TIMS) at GEOMAR with both instruments operating in static multi-collection. Sr and Nd isotopic ratios are normalized within run to  $^{86}\text{Sr}/^{88}\text{Sr} = 0.1194$  and  $^{146}\text{Nd}/^{144}\text{Nd} = 0.7219$ , respectively. All Sr isotope data are reported relative to NBS987  $^{87}\text{Sr}/^{86}\text{Sr} = 0.710250$  with an external 2 SD = 0.000012 (N = 20) for the MAT262 and 2 SD = 0.000009 (N = 12) for the TRITON. The Nd isotope data are reported relative to La Jolla  $^{143}\text{Nd}/^{144}\text{Nd} = 0.511849 \pm 0.00005$  (N = 27, 2 SD). The long-term NBS 981 values are  $^{206}\text{Pb}/^{204}\text{Pb} = 16.898 \pm 0.006$ ,  $^{207}\text{Pb}/^{204}\text{Pb} = 15.437 \pm 0.007$ ,  $^{208}\text{Pb}/^{204}\text{Pb} = 36.527 \pm 0.024$  (N = 125, 2 SD) and corrected to the NBS 981 values given in Todt et al. (1996) [28]. Total chemistry blanks were  $<100$  pg for Sr, Nd, and Pb, and thus considered negligible.

### 3. Results

#### 3.1. Morphology

Hydrographer Ridge, located in the North Iturup transverse zone of the Kurile Island Arc, is a ~20 km long, WNW–ESE-trending ridge structure rising up to ca. 1600 m above the 3000–3500 m deep floor of the Kurile Basin. According to Avdeiko et al. (1992) [14] the ridge represents a chain of three volcanoes marked in the catalogue of submarine volcanoes of the Kurile Arc as 7.12, 7.13, and 7.14. A single beam bathymetric and seismic survey conducted on cruise LV 29 were carried out only at volcano 7.12. (Figure 2). The eastern area of volcano 7.12. shows a cross section of a typical stratovolcano with its top tilting to the north towards the Kurile Basin center, interpreted as resulting from the subsidence of the Kurile Basin (Avdeiko et al., 1992; Baranov et al., 2002b [14,17]). The base of the volcano 7.12 is covered by horizontally layered sediments of the Kurile Basin with a thickness

of 800–1000 m. In some areas of the volcano's slopes, the recording of seismic signals disappears due to their scattering on structures such as peripheral cones or extrusion domes. One of these cones with a height of about 200 m was discovered at a distance of 4 km to the west of the volcano's summit (Figure 2).

The three Sonne Volcanoes (referred to here as southern, central and northern Sonne Volcano) are aligned along a N–S-striking line (Figure 3). The distance between the northern and southern volcano amounts to 55 km. The base of all volcanic edifices is covered by sediments with a thickness of 1–1.5 km (Karp et al., 2003 [29]), and only their tops rise 150–300 m above the sea floor.

The southern Sonne Volcano is located on the lower Kurile Basin slope in about 2500 m water depth (Figure 3a). Its top is elongated in N–S direction and has basal dimensions of about  $2.5 \times 4$  km. A prominent hill with a steep southern flank marks the northern edge of the volcano. An OFOS (ocean floor observation system) survey and dredging revealed that the top of this volcanic edifice represents remnants of a collapsed crater-like structure which consists of layered volcanoclastic rocks, most likely indicating explosive eruptions. This may suggest that the volcano was formed at shallower water depths than its present depth, being consistent with significant subsidence of the Kurile Basin as, for example, postulated by Baranov et al. (2002b) [17].

The central and northern Sonne Volcanoes are located on the upper Kurile Basin slope in 1500–1750 m water depth. The central volcano forms a ~300 m high and ~6.5 km long ridge-like structure which strikes in NE–SW direction at slight oblique angle to the overall alignment of the Sonne Volcanoes. A steep fault scarp, striking parallel to the axis of the central volcano, cuts its southeastern side (Figure 3b). The northern volcano is located 22 km to the north of the central volcano. The top of this volcanic edifice consists of three peaks being up to ~3.5 km in diameter and ~300 m high (Figure 3c). Around the central and northern volcanoes, very prominent moats with depths up to 100 m have been formed by oceanic currents around the basement outcrops.

### 3.2. Sampling and Petrography

Dredge haul LV29-126-1 (~2500 to 2000 m below sea level (b.s.l.), Figure 2) on the southern slope of the western Hydrographer Ridge (volcano 7.12) yielded ca. 100 kg angular fragments of homogeneous pillow-like lava. The homogeneity, angular shape, and rough, freshly broken surfaces of the dredged rocks strongly indicate that they are fragments of a (pillow)-lava flow once formed by an eruption of this volcano, i.e., they represent in situ rocks. The lava fragments are highly porphyric (up to 5–10 vol.% phenocrysts) and slightly vesicular with rounded to oval-shaped vesicles being commonly being 1–3 mm in diameter. Major phenocryst phases comprise plagioclase, olivine, clinopyroxene, amphibole, and Fe-Ti-oxides; orthopyroxene occurs minor. The groundmass shows a microlitic texture and consists of glass with numerous plagioclase microlites and varying amounts of clinopyroxene, amphibole and Fe-Ti-oxides (Werner et al., 2003 [30]). The phenocrysts and the groundmass of these rocks are fresh or show only minor alteration. Besides numerous fragments of slightly lithified diatomaceous sedimentary rocks, dredge haul LV29-126-4, carried out ca. 3 nm west of LV29-126-1 (Figure 2), recovered a porphyric, vesicular lava block (ca.  $25 \times 30$  cm in size) which also show evidence for an in situ origin. Major phenocrysts of the lava are olivine, orthopyroxene, clinopyroxene, and plagioclase. The lava is only minor affected by alteration with the exception of the olivine phenocrysts which are partially replaced by secondary minerals. A noteworthy feature of this lava are common glomerophytic clusters of gabbroic (cpx + plag) and wehrlitic (ol + cpx ± plag) rock fragments, which are considered to be the enclaves of crystal cumulates (Werner et al., 2003 [30]).

Even though sampling of the Sonne Volcanoes proved very difficult because of their gentle slopes, thick sediment cover, Fe-Mn encrustations and poor weather conditions, two dredge hauls carried out on the steep fault scarp of central Sonne Volcano (Figure 3b) yielded lava fragments suitable for radiometric age dating and geochemical analyses. Dredge haul SO178-7-1 contained up to 25 cm large fragments of porphyritic lava with a fine-grained or microcrystalline matrix. The homogeneity of the dredged rocks and their angular shape clearly indicate that they represent in situ rocks. Phenocrysts (<5–7%) are plagioclase (<2–3 mm), clinopyroxene, and olivine (<0.5 mm). The groundmass consists of plagioclase microlites together with variable amounts of olivine,

clinopyroxene, Fe-Ti-oxides and altered glass (Werner et al., 2004 [31]). Although all rock fragments are covered with ~2-3 cm thick manganese crusts, groundmass and phenocrysts of the lava are fairly fresh except for the olivine phenocrysts which are completely replaced by iron hydroxides. A very similar, ~23 cm long angular fragment of olivine-clinopyroxene-plagioclase-bearing basalt was obtained by dredge haul SO178-83-1 from the northern part of the scarp. This lava is more intensely altered than the rocks from dredge SO178-7-1 (Werner et al., 2004 [31]).

### 3.3. Ar/Ar Age Dating

Three samples from the Hydrographer Ridge and from the central Sonne Volcano have been dated and geochemically analyzed (Tables 1–3). Multiple laser  $^{40}\text{Ar}/^{39}\text{Ar}$  analyses of single hornblende crystals from the Hydrographer Ridge samples yielded uniform ages of  $3.17 \pm 0.10$ ,  $3.29 \pm 0.19$ , and  $3.31 \pm 0.09$  Ma (Figure 4A; Table 1), which fall in the age range of the volcanoes of the recent Kurile Island Arc. Significantly older ages of  $25.30 \pm 0.54$ ,  $25.86 \pm 0.60$ , and  $25.83 \pm 0.55$  Ma were determined for the samples from the central Sonne Volcano by analyses of single feldspar crystals (Figure 4B; Table 1), indicating that the Sonne Volcanoes were formed in a very early stage of the formation of the Kurile Basin.

**Table 1.** Results of single-crystal  $^{40}\text{Ar}/^{39}\text{Ar}$  analyses.

Sample Number	Mineral Phase	Weighted Mean Age (Ma) (2s Error)	Mean Square Weighted Deviate (MSWD)	Probability	Number of Single-Crystal Analyses
<b>Hydrographer Ridge:</b>					
LV29 126-1-1	hbl	$3.17 \pm 0.10$	0.94	0.53	19
LV29 126-1-2	hbl	$3.31 \pm 0.09$	0.87	0.62	19
LV29 126-4-1	hbl	$3.29 \pm 0.19$	0.61	0.88	17
<b>Central "Sonne Volcano":</b>					
SO178 DR7-1-1	fsp	$25.30 \pm 0.54$	0.95	0.49	12
SO178 DR7-1-2	fsp	$25.86 \pm 0.60$	1.20	0.26	12
SO178 DR83-1-1	fsp	$25.83 \pm 0.55$	1.17	0.30	12

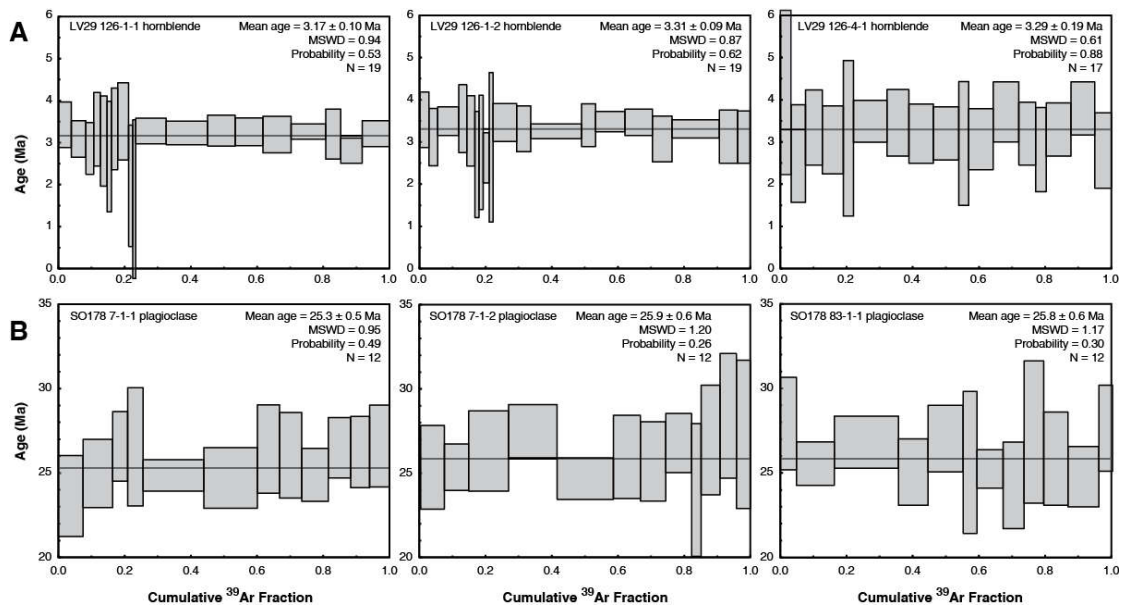


**Figure 4.**  $^{40}\text{Ar}/^{39}\text{Ar}$  analyses of (A) hornblende phenocrysts from samples LV 126-1-1, LV 126-1-2, and LV 126-4-1 (Hydrographer Ridge) and (B) plagioclase phenocrysts from samples SO178 DR7-1-1, DR7-1-2, and DR83-1-1 (central “Sonne Volcano”). Single-crystal age spectra in order of analysis; single-crystal ages (2 sigma error bars) versus cumulative  $^{39}\text{Ar}$  fraction. MSWD = Mean Square Weighted Deviates ( $\text{SumS}/\text{N}-1$ ). Probability from Chi-Square tables. N = Number of single-crystal analyses. Diagrams generated with Isoplot 3 (Ludwig 2003 [32]).

### 3.4. Geochemistry

Major and trace element analyses (Table 2) reveal hawaiitic to trachy-andesitic compositions for Hydrographer Ridge pillows ( $\text{SiO}_2 = 50.6\text{--}67.3$  wt.%,  $\text{MgO} = 3.1\text{--}3.5$  wt%) and very uniform, trachytic compositions for the Sonne Volcano lavas (Figure 5;  $\text{SiO}_2 = 59.5\text{--}60.2$  wt.%,  $\text{MgO} < 0.5$  wt%). Despite their age and submarine eruption, the samples are surprisingly fresh with  $\text{H}_2\text{O} \leq 1.4$  and almost no  $\text{CO}_2$ . The Mg values (Mg#) vary from 0.51 to 0.63 for Hydrographer Ridge. The Mg# of the Sonne Volcano lavas are rather low with 0.12–0.14, reflecting their evolved (trachytic) nature. Accordingly, only trace element contents and radiogenic isotopes are used in the following to characterize their magma sources, since in particular the Sr-Nd-Pb-isotope ratios are not affected by differentiation processes.

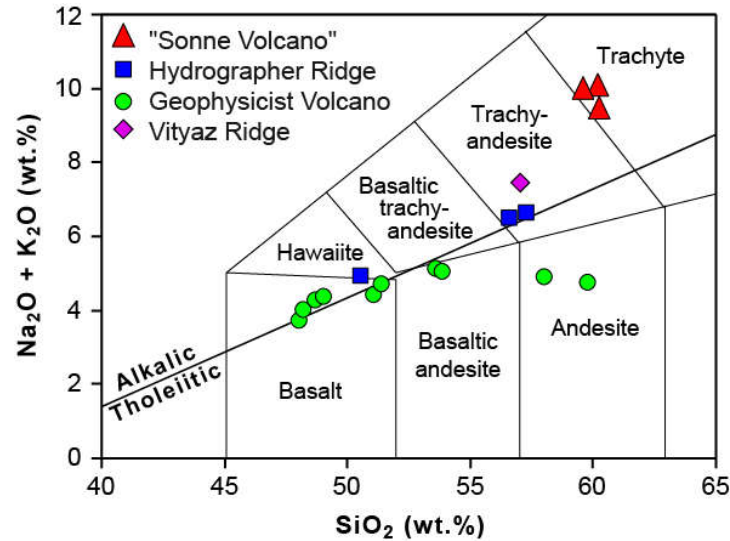


**Figure 5.** Major element data of whole rock samples from Hydrographer Ridge and the central Sonne Volcano illustrated by a total alkali-silica diagram after Le Bas et al. (1986) [33]. Samples from Geophysicist Volcano (Baranov et al., 2002b) [17] and Vityaz Ridge (Leikov et al., 2008) [15] are shown for comparison.

All samples from both volcanoes show relative enrichment of fluid-mobile elements (e.g., Rb, Ba, and U) and relative depletion of fluid-immobile elements (e.g., Nb, Ta, and Zr), as is characteristic for arc lavas, in particular those from the Kurile Island Arc (Figure 6a). The Sonne Volcano trachytes, however, show a significant enrichment in most trace elements but a remarkable depletion in Sr compared to the Kurile Island Arc. The rare earth element (REE) patterns on chondrite-normalized diagrams show a significant enrichment in light REE's (Figure 6b), as is characteristic for high-K calc-alkaline subduction zone volcanic rocks. The Sr-Nd-Pb isotopic compositions of the analyzed samples from Sonne Volcano and Hydrographer Ridge display a narrow compositional range regardless of their petrography and show little variation in most isotope ratios (Figure 7a,b; Table 3). Their  $^{87}\text{Sr}/^{86}\text{Sr}$  (0.70285–0.70318),  $^{143}\text{Nd}/^{144}\text{Nd}$  (0.51296–0.51305) and  $^{207}\text{Pb}/^{204}\text{Pb}$  ratios (15.46–15.48) fall into the range of the Kurile Island Arc. The  $^{206}\text{Pb}/^{204}\text{Pb}$  (18.04–18.10) and  $^{208}\text{Pb}/^{204}\text{Pb}$  ratios (37.86–37.93) of the central Sonne Volcano, however, are less radiogenic than those of the Kurile Island Arc rocks. Similar lead isotopic compositions have been observed in samples from Geophysicist volcano (Figure 7b), which is considered to be a Kurile back arc volcano situated on thinned continental crust (Baranov et al., 2002b [17]).

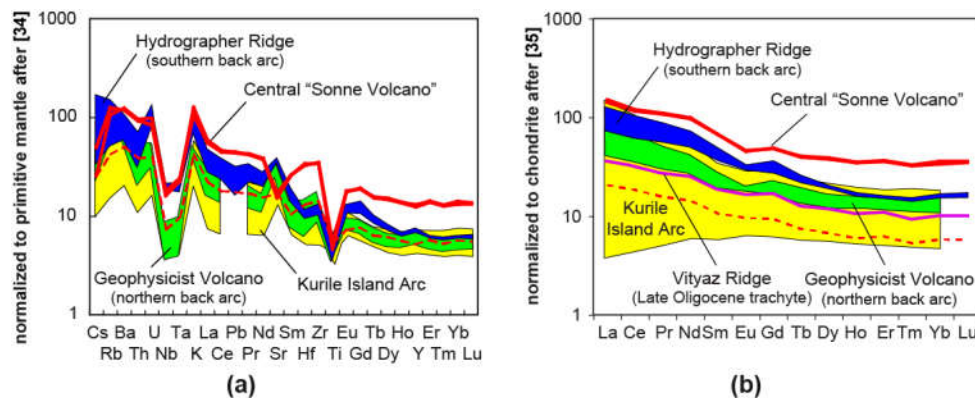


**Figure 6.** (a) Multi element diagram after Hofmann (1988) [34] and (b) Rare Earth Element (REE) patterns after McDonough & Sun (1995) [35] of the central Sonne Volcano trachytes (red lines)

compared to data from the Hydrographer Ridge (blue field) and Geophysicist back arc volcanoes (green field), the Kurile Arc (yellow field), and a Vityaz Ridge trachy-andesite (purple line, only shown in b). The enrichment in most trace elements of the Sonne Volcano trachytes compared to the Kurile Arc reflects enrichment due to differentiation (crystal fractionation) and contamination by continental material. The dashed red lines show the composition of the “Sonne Volcano” trachytes if normalized to the average Yb content (5.86) of the present Kurile Island Arc lavas. Note that the normalized trace element patterns fall in the field for the Kurile Arc. Kurile Arc data after Bindeman and Bailey (1999), Hoernle et al. (2000), Martynov et al. (2010 a, b, 2015), Martynov (2013), Martynov and Martynov (2017) [36–42] and unpublished data of Hoernle and Werner; data for Geophysicist Volcano from Baranov et al. (2002b) [17] and data for Vityaz Ridge trachy-andesite are from Lelikov et al. (2008) [15].

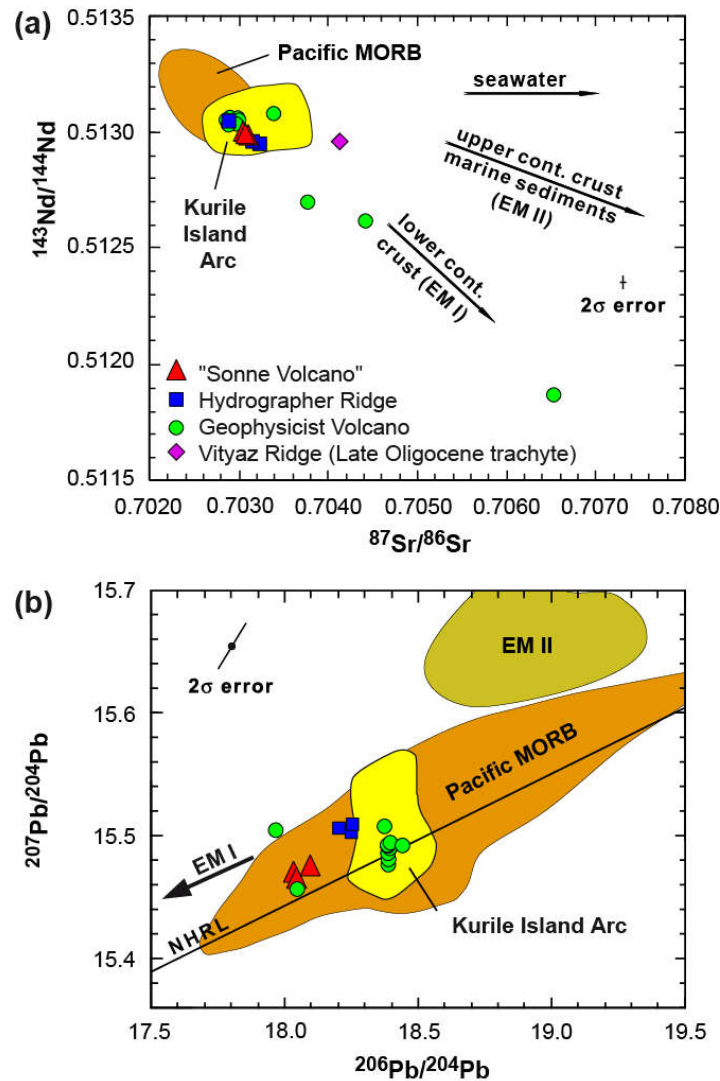


**Figure 7.** (a)  $^{87}\text{Sr}/^{86}\text{Sr}$  versus  $^{143}\text{Nd}/^{144}\text{Nd}$  and (b)  $^{206}\text{Pb}/^{204}\text{Pb}$  versus  $^{207}\text{Pb}/^{204}\text{Pb}$  (uranogenic Pb) isotope correlation diagrams. Whereas the isotope signatures of Hydrographer Ridge overlap completely with the fields for the Kurile Island Arc, the  $^{206}\text{Pb}/^{204}\text{Pb}$  and  $^{208}\text{Pb}/^{204}\text{Pb}$  ratios of the rocks from the central Sonne Volcano extend towards lower continental crust, indicating contamination by lower continental crust and/or subcontinental lithospheric mantle with a composition similar to the enriched mantle one (EM I) component. The Late Oligocene trachy-andesite from the Vityaz Ridge show  $^{143}\text{Nd}/^{144}\text{Nd}$  ratios similar to those of Sonne Volcano and Hydrographer Ridge but show elevated  $^{87}\text{Sr}/^{86}\text{Sr}$  indicating most likely seawater alteration. Data sources for Kurile Arc and Geophysicist

Volcano as in Figure 6, data from Vityaz Ridge from Emelyanova et al. (2012) [16], EM I and EM II are after Zindler and Hart (1986) and Hart et al. (1992) [43,44]. Fields for Pacific MORB are from PetDB data base (<http://www.earthchem.org/petdb>) based on analyses of fresh glass.

**Table 2.** Major and trace element compositions.

	Hydrographer Ridge			Central "Sonne Volcano"			
	LV29 126-1-1	LV29 126-1-2	LV29 126-1-2 Replicate	LV-29 126-4-1	SO178 DR7-1-1	SO178 DR7-1-2	SO178 DR83-1-1
Major elements in weight percent (wt.%)							
SiO <sub>2</sub>	57.29	56.59		50.61	59.5	60.06	60.14
TiO <sub>2</sub>	0.63	0.64		1.07	0.83	0.86	0.97
Al <sub>2</sub> O <sub>3</sub>	17.33	17.40		19.90	19.39	19.44	19.22
Fe <sub>2</sub> O <sub>3</sub>	6.16	6.34		7.30	5.67	5.74	5
MnO	0.16	0.16		0.12	0.13	0.16	0.09
MgO	3.12	3.30		3.46	0.34	0.41	0.38
CaO	6.73	6.93		11.40	3.12	3.11	3.36
Na <sub>2</sub> O	3.65	3.60		3.15	6.03	6.03	6.06
K <sub>2</sub> O	2.98	2.88		1.79	3.82	3.91	3.25
P <sub>2</sub> O <sub>5</sub>	0.38	0.39		0.39	0.28	0.3	0.31
SUM	98.43	98.23		99.19	99.11	100.02	98.78
H <sub>2</sub> O	1.34	1.41		0.92	0.73	0.81	0.63
CO <sub>2</sub>	0.01	0.01		0.02	0.03	0.02	0.01
Total	99.78	99.65		100.13	99.87	100.85	99.42
Mg# *	0.53	0.53		0.51	0.12	0.14	0.14
Trace elements in parts per million (ppm)							
Li	5.85	6.46	6.40	4.33	8.49	9.80	7.52
Sc	14.3	14.1	14.2	32.8	15.2	15.0	14.5
V	161	152	154	296	38.4	38.4	55.5
Cr	36.2	28.4	28.1	222	0.89	0.50	0.805
Co	15.2	15.1	15.1	19.6	3.78	4.53	3.77
Ni	13.8	15.0	14.9	27.1	41.8	59.4	32.4
Cu	16.7	18.8	18.6	46.2	8.02	9.24	4.63
Zn	67.7	66.1	64.8	72.1	93.9	121	89.0
Ga	18.9	18.1	18.1	19.3	23.1	22.8	21.9
Rb	85.5	79.4	78.5	26.8	64.4	67.0	56.3
Sr	685	677	676	713	276	282	309
Y	28.2	27.7	27.4	26.9	48.4	51.2	50.5
Zr	141	124	123	98.5	330	328	337
Nb	12.8	12.0	11.9	11.2	9.90	9.93	11.1
Mo	2.21	2.13	2.16	1.42			
Sn	0.92	0.86	0.85	0.89			
Sb	0.12	0.10	0.10	0.09			
Cs	4.53	4.39	4.34	0.88	1.32	1.32	0.69
Ba	600	570	569	354	715	712	747
La	29.4	28.9	28.6	17.0	34.2	35.9	33.5
Ce	62.3	61.7	61.1	37.7	72.4	73.7	70.6
Pr	8.18	8.08	8.02	5.24	10.0	10.3	10.1
Nd	33.0	32.8	32.5	22.9	44.0	45.6	45.1
Sm	7.22	7.32	7.23	5.33	9.82	9.91	9.98
Eu	1.85	1.87	1.85	1.59	2.56	2.53	2.60
Gd	7.10	7.08	7.09	5.40	9.56	9.78	9.61
Tb	0.94	0.95	0.93	0.78	1.42	1.43	1.46

Dy	5.01	5.01	4.91	4.60	9.33	9.27	9.59
Ho	0.93	0.93	0.91	0.91	1.91	1.92	1.95
Er	2.54	2.50	2.46	2.55	5.70	5.77	5.88
Tm	0.38	0.37	0.36	0.37	0.81	0.81	0.83
Yb	2.63	2.54	2.48	2.49	5.40	5.49	5.79
Lu	0.40	0.38	0.38	0.37	0.84	0.85	0.86
Hf	3.39	3.06	3.02	2.48	8.96	8.99	8.64
Ta	0.76	0.70	0.70	0.61	0.79	0.79	0.84
Tl	0.91	0.90	0.88	0.26	0.46	0.43	0.36
Pb	5.44	5.46	5.35	2.78	7.77	7.63	7.57
Th	5.20	5.10	4.98	2.33	7.44	7.48	7.75
U	1.84	1.79	1.78	2.68	1.71	1.68	1.98

\* Mg values were calculated according to the formula  $Mg\# = (MgO/40.32)/((MgO/40.32) + ((Fe_2O_3 \text{ (Total)}/79.8)*0.9))$  after Harvey et al. (2006) [45].

**Table 3.** Sr-Nd-Pb-isotope data.

	Hydrographer Ridge			Central "Sonne Volcano"			
	LV29 126-1-1	LV29 126-1-2	LV-29 126-4-1	SO178 DR7-1-1	SO178 DR7-1-2	SO178 DR83-1-1	
<sup>87</sup> Sr/ <sup>86</sup> Sr	0.703149	0.703178	0.702850	0.703145	0.703144	0.703174	
2 SE	0.000003	0.000002	0.000003	0.000005	0.000005	0.000005	
<sup>143</sup> Nd/ <sup>144</sup> Nd	0.512974	0.512956	0.513053	0.512990	0.512989	0.512979	
2 SE	0.000002	0.000002	0.000003	0.000002	0.000002	0.000001	
<sup>206</sup> Pb/ <sup>204</sup> Pb	18.367	18.373	18.325	18.044	18.043	18.096	
2 SE	0.0004	0.0004	0.0004	0.001	0.001	0.001	
<sup>207</sup> Pb/ <sup>204</sup> Pb	15.478	15.481	15.474	15.466	15.464	15.475	
2 SE	0.0004	0.0004	0.0004	0.001	0.001	0.001	
<sup>208</sup> Pb/ <sup>204</sup> Pb	38.110	38.121	38.058	37.867	37.860	37.929	
2 SE	0.0011	0.0012	0.0009	0.002	0.002	0.001	

## 4. Discussion

### 4.1. Opening and Early Evolution of the Kurile Basin

The Kurile Island Arc once started to develop on continental crust (Sergeev 1976, Zlobin 1987, Zonenshain et al., 1990, Verzhbitsky and Kononov 2010; Emel'yanova et al., 2012 [16,46–49]). The ~1 My. old Geophysicist back arc volcano, located on the abyssal plain of the Kurile Basin ~100 km behind of the northern part of the Kurile arc volcanic front (Figure 1), is accordingly located on thinned, submerged continental crust (Baranov et al., 2002b [17]). The ~3.3 My. old Hydrographer Ridge is the outermost back arc volcano of the southern Kurile Island Arc and therefore represents some kind of southern equivalent to the Geophysicist Seamount (Figure 1). By contrast to the Geophysicist Seamount, the lavas of Hydrographer Ridge do not show geochemical evidence for contamination by continental material (cf. Figures 6 and 7), which could suggest that this volcano is most likely located on arc or oceanic crust and that continental crust does not exist in this part of the arc. This may indicate that either former continental crust has been completely transformed to arc crust in this part of the back arc or that Hydrographer Ridge is located on oceanic crust formed by back arc spreading.

The Sonne Volcanoes are located on the opposite side of the Kurile Basin on continental crust (further from the present-day Kurile Arc). This is most likely reflected by the isotopic variations of their lavas, which indicate assimilation of a lower continental crustal and/or an enriched subcontinental lithospheric mantle (EMI-type) component (Figure 7b). The ascent of the Sonne Volcanoes magmas through and probable stagnation in continental crust can also explain the trachytic composition and the, in particular lower Pb, isotopic characteristics of the rocks. Their relative depletion in Sr, Eu and Ti (Figure 6a) probably results from fractional crystallization of

plagioclase and Ti-oxides, respectively, from the Sonne Volcanoes magmas during stagnation in the crust. The relative enrichment in most other trace elements is primarily due to incompatible element enrichment during melt differentiation as well as some contamination by continental material. In this respect it is important to note that the trace element patterns of the Sonne Volcano lavas fall completely in the field of the Kurile Island Arc if normalized to an average value of a less incompatible trace element of the Kurile Island Arc rocks as, for example,  $Yb = 5.86$  (Figure 6a).

Trace element ratios, such as La/Yb, La/Sm and Sm/Yb, and Sr, Nd and  $^{207}Pb/^{204}Pb$  isotopic signatures of the Sonne Volcanoes are very similar to those of the Kurile Island Arc (Figures 6–8), indicating the same or at least a similar magma source for the 26 My. old Sonne Volcanoes and the present Kurile Island Arc. Therefore the Sonne Volcanoes represent ancient Kurile Island Arc volcanoes presently located 300–350 km from the volcanic front on the northwestern Kurile Basin margin (Figure 1). Considering that the distance between the volcanic front and the outermost young back arc volcanoes (e.g., Geophysicist Seamount or Hydrographer Ridge; Figure 1) of the Kurile Island Arc does not exceed ~100 km, the Sonne Volcanoes have migrated at least 200 km since their formation at ~26 Ma, if the angle of subduction has not changed significantly. This change in location must have been connected with the Kurile Basin opening through rifting and seafloor spreading. The age of the Sonne Volcanoes implies that the Kurile Island Arc was active as far back as the Oligocene and provides a maximum age for the opening of the Kurile Basin.

Some years ago, a previously unknown extensional structure in the Kurile Island Arc system was discovered in the frontal part of the central Kuriles (Laverov et al., 2006; Kulinich et al., 2007) [50,51], hereafter referred to as Kurile Fore Arc Extension Structure (KFES). This extensional structure splits the outer high (Vityaz Ridge) in two parts (Figure 1). Due to stretching of the crust, the seafloor of this feature has been submerged by 2–3 km relative to the top of Vityaz Ridge and consists of tilted blocks. It is bounded by the NW–SE striking Bussol Graben to the southwest and by two fault scarps of the Vityaz Ridge to the northeast. Therefore it has the fan-like shape opening towards the trench. The uniform volcanogenic and volcano-sedimentary complex was dredged on the lower scarp of the Vityaz Ridge in water depths of 1500–2000 m (Figure 1). The samples yielded by dredging comprise trachytic, trachy-andesitic, and trachy-rhyolitic lavas and tuffs, conglomerates and coarse sandstones (Lelikov et al., 2008) [15]. K/Ar dating of a Vityaz Ridge trachy-andesite and spore-pollen analysis of the associated sedimentary rocks yielded a Late Oligocene age (27.5 Ma, Lelikov et al., 2008 [15]) for this complex which is almost identical to the Ar/Ar ages of the central Sonne Volcano. The 27.5 My. old trachy-andesitic lava is geochemically similar to the Sonne Volcano lavas and falls into the field for the Kurile Island Arc (Figures 6b and 8), suggesting that these features may have originated contemporaneously from a common source. Considering that the Kurile Arc started to form on continental crust, it may be expected that the Vityaz Ridge trachy-andesite shows similar characteristics of continental contamination as the Sonne Volcano. According to seismic refraction data, however, the Vityaz Ridge has a crustal thickness of only ~20 km compared to 30–35 km of the continental Kurile Island Arc crust (Zlobin et al., 2008 [47]). Zonenshain et al. (1990) and Verzhbitsky and Kononov (2010) [48,49] propose that the Vityaz Ridge was part of a Mesozoic intra-oceanic island arc which has been accreted to the Kurile Arc.

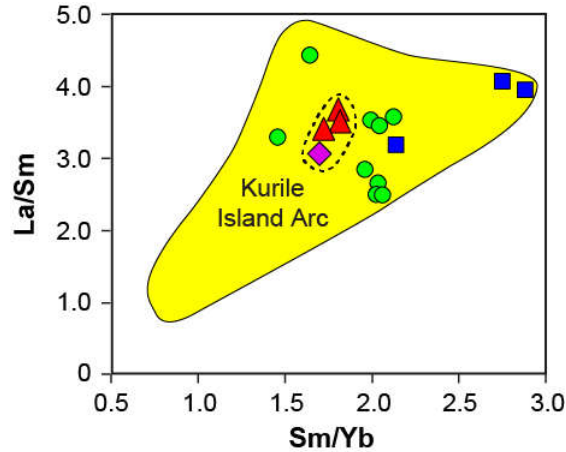


**Figure 8.** Trace element ratios exemplified by La/Sm versus Sm/Yb illustrate very similar trace element signatures for the central “Sonne Volcano” and the Late Oligocene trachy-andesites from the fore arc extension structure on Vityaz Ridge (illustrated by the dashed line) which fall within the field of the present Kurile Island Arc, pointing towards derivation from a common source. Data sources as in Figure 6, symbols as in Figure 7.

The similar age of the Sonne Volcanoes and Vityaz Ridge and similar REE composition, however, suggests that the Vityaz Ridge formed as part of the ancestral Kurile Arc. The formation of the Vityaz fore arc complex probably corresponds to the beginning of the extension in the fore arc area, suggesting that the processes of subduction, Kurile Basin opening and frontal arc extension occurred synchronously. According to this observation, the opening process in the rear part and extension in the frontal part of the Kurile Island Arc must have been triggered by the same mechanism.

To identify this mechanism, we will consider two models for the evolution of the Kurile back arc basin. The first model attributes the opening of the Kurile Basin to a southward migration of the eastern half of Hokkaido and of the Proto-Kurile Island Arc (Jolivet 1987; Maeda 1990 [3,4]). This migration was considered to result from dextral displacement along the Sakhalin–Hokkaido shear zone, which extends over a distance of 2000 km from northern Sakhalin to Hokkaido (Figure 9, Jolivet 1987 [3]).

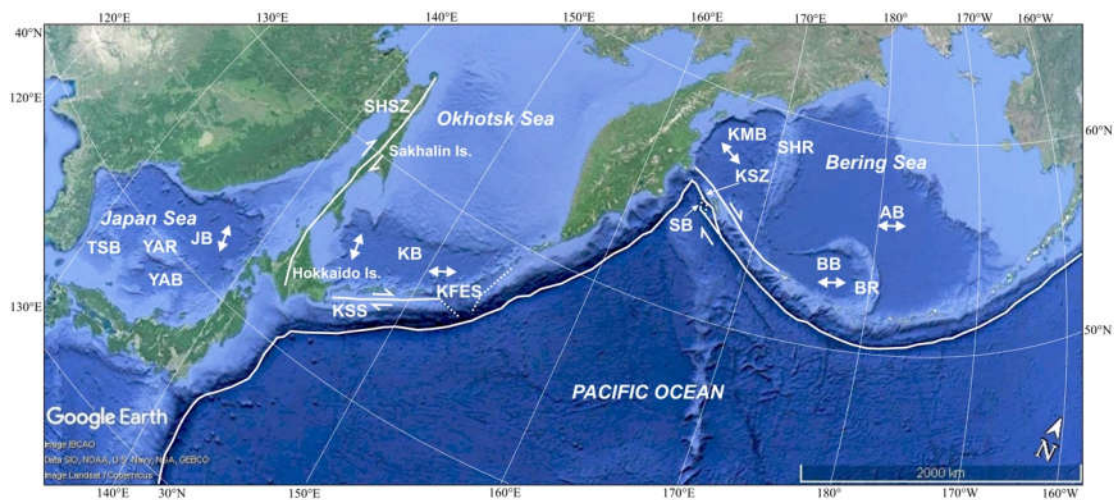


**Figure 9.** Marginal seas of the NW Pacific and their back arc basins: AB—Aleutian, BB—Bowers, KMB—Komandorsky, KB—Kurile, JB—Japan, YAB—Yamato, TSB—Tsushima. Ridges and rises

separating the back arc basins: BR—Bowers, SHR—Shirshov, YAR—Yamato. Extension structures in the Aleutian and Kurile fore arcs: SB—Steller Basin (Baranov et al., 1991 [52]), KFES—Kurile Fore Arc Extension Structure (Laverov et al., 2006 [50]). The white line marks the trench axis, white lines with arrows indicate active shear zones: KSZ—Komandorsky (Baranov et al., 1991 [52]), SHSZ—Sakhalin–Hokkaido (Jolivet et al., 1987 [3]), KSS—Kurile Sliver Shear (Kimura 1986 [53]). White lines with arrows at both ends mark the opening direction of the back arc basins. Two opening directions are suggested for the Kurile Basin: NNW–SSE direction in Middle Miocene and NE–SW direction later than Late Miocene (TuZino and Muramaki 2008 [54]).

Displacements along this NS-striking shear zone began in Oligocene–Miocene and continue to the present. The opening of the Kurile Basin was governed by dextral displacement along this shear zone (Fournier et al., 1994 [55]). The spreading axis in the Kurile Basin should be orthogonal to this shear zone and maximum extension has occurred in the western Kurile Basin. In this case the Kurile Basin will have the shape of a triangle with the vertex facing to the east. However, the KFES expands to the north and its vertex faces to the south (Figure 9), and this geometry cannot be explained with this model.

The second model suggests that the spreading axis in the Kurile Basin strikes N–S orthogonal to the general orientation of the basin. This spreading structural pattern is based on seismic studies which revealed a NS-striking basement rise, being completely covered by sediments, in the central part of the Kurile Basin on a traverse of the Friza Strait (Figure 1; Gribidenko et al., 1995; Baranov et al., 2002a [5,6]). The morphology of this basement rise is characterized by symmetrical volcanic edifices on the rise axis and faulted blocks which tilt in opposite directions on the flanks. Such structural pattern could be interpreted as a fossil spreading center, implying an opening direction of the Kurile Basin parallel to the general trend in NE–SW-direction (Baranov et al., 2002a [6]). In this model, spreading in the Kurile Basin and extension in the Kurile fore-arc were presumably connected with dextral displacement along a NE–SW-striking shear zone which could have been formed together with the Kurile subduction zone. In this case, the maximum extension in the Kurile Basin and KFES should be confined to their southern and northern parts, respectively.

Assuming an opening in NNW–SSE-direction (first model), the shift of the Sonne Volcanoes, measured from the outermost back arc volcanoes to the northernmost Sonne Volcano amounts to 230 km (Figure 1), whereas opening and spreading of the basin in NE–SW-direction (second model) would imply a larger shift of 360 km. The Kurile Basin is presently not actively spreading and there is no clear evidence when the spreading ceased. Based on the assumption of a minimum age of 8 Ma (Late Miocene) as suggested by Takeuchi et al. (1999) and Ikeda et al. (2000) [12,13], the spreading rates have been rather slow at 1.3 cm/y and 1.8 cm/y for the first and second model, respectively.

The Kurile Basin currently subsides at a rate of about 0.5–2 mm/year (Baranov et al., 2002b [17]). The recent stress field of the Kurile Basin, inferred from the analysis of seismic activity, focal mechanism solutions and the structure of the sedimentary cover, suggests that compression is responsible for its rapid subsidence and that subsidence may be an important step in the transition from basin formation to its destruction (Baranov et al., 2002b [17]).

#### 4.2. Comparison of General Characteristics of the Back Arc Basins Along the Eastern Margin of Eurasia

The Kurile back arc basin is one of the back arc basins of the Western Pacific Ocean which form a chain extending from north to south over a distance of about 12,000 km. In the following we first provide an overview of structure, age and evolution of the back arc basins in the Bering and Japan Seas (Figure 9) and then compare their major features with those of the Kurile Basin.

The western Bering Sea consists of the Aleutian, Bowers and Komandorsky back arc basins (Figure 9). The Aleutian and Bowers basins are located in the rear of the eastern and central Aleutian island arc and the Komandorsky Basin is situated in the rear of its western segment, which is a transform fault (Cormier 1975; Baranov et al., 1991; Seliverstov 1998 [52,56,57]). The velocity structure of the Aleutian Basin crust has an oceanic affinity (Barth et al., 2012 [58]), but its composition and age remain uncertain since its basement has not been sampled. Distinct N–S magnetic anomalies in the Aleutian Basin reveal Early Cretaceous (Chronos from M1 to M13) and apparently Early Tertiary ages

(Cooper et al., 1977; Cooper et al., 1992 [59,60]). The Early Tertiary anomalies are confined to the Vitus Arch, a 100–200 km wide basement uplift that crosses the Aleutian Basin from southwest to northeast. The Vitus Arch is considered to be a fossil spreading center (Cooper et al., 1992 [60]). A new magnetic compilation revealed the presence of well-defined N–S stripes in the Aleutian Basin, which could have formed during sea-floor spreading at a mid-ocean ridge or back arc spreading center. However, these anomalies are not sufficiently symmetrical and their sequence cannot be correlated to the geomagnetic polarity timescale (Scheirer et al., 2013 [61]).

Two major models have been proposed for the formation of the Aleutian Basin. According to the first, the Aleutian Basin crust was trapped when the subduction zone “jumped” from the Beringian margin to its present location (Scholl et al., 1975; Cooper et al., 1977 [59,62]). This probably occurred c. 50–47 My. ago in response to a change in the Pacific Plate motion from NNW to WNW, which is reflected by the distinct bend of the Hawaiian-Emperor seamount chain (Sharp and Clague 2006 [63]). The oldest age from the Aleutian Arc is 46 Ma (Jicha et al., 2006 [64]) and coincides within error with the time of the change in Pacific Plate motion.

The second model assumes that the Aleutian Basin opened as a result of back arc spreading. In accordance with this scenario, the Beringian Arc never shut down, but rotated southward resulting in the opening the Aleutian Basin. Back arc spreading in the Aleutian Basin may have been related to trench rollback due to changes in the motion of the Pacific plate (Stern et al., 2012 [65]). It is also assumed that the Aleutian Basin, similar to most of the back arc basins in the western Pacific, was formed as a result of dextral pull-apart in Paleogene (Xu et al., 2014 [66]).

The Bowers Basin is located in the rear of the Bowers Ridge (Figure 9) and shows distinct, N–S striking magnetic anomalies for which an Early-Tertiary or older age is assumed (Scholl 2007 [67]). Bowers seamount dated at 22–24 Ma is believed to have formed during the opening of the Bowers back arc basin (Wanke et al., 2012) [68].

Bowers Ridge extends from the Central Aleutian Arc to the north, where it bends westward and fades into a WSW-striking chain of seamounts which extends towards the southern end of the Shirshov Ridge (Figure 9). Multichannel seismic profiling data reveal a high (up to 7 km) thickness of the sedimentary cover along the northern border of the Bowers Ridge, which indicates the presence of subduction of the oceanic crust of the Aleutian Basin along the northern edge of the Bowers Ridge during the Cretaceous and Early Paleogene (Cooper et al., 1981 [69]). Bedrocks dredged from the Bowers Ridge show island arc affinity and  $^{40}\text{Ar}/^{39}\text{Ar}$  dating yielded an Oligocene ages (26–32 Ma) for these samples (Wanke et al., 2012 [68]). The Oligocene age of the rocks implies that Bowers Ridge was formed after the initiation of subduction along the Aleutian trench (c. 46 Ma; Jicha et al., 2006 [64]) and isolation of the Aleutian Basin from the Pacific.

These data are consistent with the formation of the Bowers subduction zone within the Bering Sea simultaneously with, or after, the formation of the Aleutian subduction zone (Cooper et al., 1981; Scholl 2007 [67,68]). Because there is no evidence for a Cenozoic spreading center within the Aleutian Basin (e.g., Scholl 2007 [67]), the Bowers subduction zone might have formed as a result of the hypothesized North Pacific Rim orogenic stream, which began in the earliest Eocene. This orogenic event involved northwestward motion of British Columbian and Alaskan crust and westward extrusion of crustal blocks into the Bering Sea, which may have triggered west-facing subduction in the Bering Sea and formation of Bowers Ridge (Redfield et al., 2007 [70]). The Bowers Basin may have formed in the rear of this subduction zone as a result of back arc spreading.

The Komandorsky Basin is located behind the western Aleutian island arc and was formed as a result of displacement along a transform fault becoming active in the Middle Eocene (Cormier 1975 [56]). The system of fossil spreading centers in this basin is oriented normal to the strike of the western Aleutian Arc and the basin formed as a pull-apart structure (Baranov et al., 1991; Seliverstov 1998 [52,57]). Linear magnetic anomalies confirm that spreading in the Komandorsky Basin continued from 20 to 10 Ma (Valyashko et al., 1993 [71]). Its termination was caused by cessation of subduction along the western boundary of the Komandorsky Basin, which originally compensated the basin spreading (Baranov et al., 1991 [52]). Presently, displacements along the Pacific/North American plate boundary are concentrated in the 150 km wide dextral Komandorsky shear zone (Figure 9). Right-

lateral motions along the fault system lead to formation of extension basins which are located both in rear and frontal parts of the arc. The largest among them is the Steller Basin which formed on the Aleutian Trench axis (Figure 9). The crustal blocks located inside this zone are displaced to the west, leading to a recent collision in the Aleutian Arc–Kamchatka junction area (Geist and Scholl 1994; Gaedicke et al., 2000 [72,73]).

The Japan Sea consists of Japan, Yamato and Tsushima deep sea basins (Figure 9). The Japan Basin is underlain by oceanic crust, the Yamato and Tsushima Basins by extended island arc crust (Tamaki 1988 [74]). Magnetic lineation identified in the Japan Basin extend along an azimuth of 70° and range in age from 27 Ma (7A) to 19 Ma (5E) (Tamaki et al., 1990 [75]). These anomalies indicate an opening of this basin in Early Miocene. They also reveal a fossil spreading center which exhibits the same trend and a possible southwestward propagation.

Deep-sea drilling in the basins of the Japan Sea has provided accurate data about the composition and age of the crust. Based on these data the evolution of these basins has been constrained from 25 Ma to the present (Jolivet and Tamaki 1992; Ingle 1992 [76,77]). Active spreading in the Japan Basins began in the Early Miocene and ended 5–10 My. ago. The Japan Sea opened as a complex pull-apart basin along a dextral shear zone that extends from Northern Sakhalin to Central Japan. Extension changed to compression at 12 Ma and the basin began to subside. The Japan Sea crust was ruptured and a juvenile subduction zone appeared along its Eastern margin at 1.8 Ma.

Taken together, the features of the back arc basins in the northwestern Pacific show that all of them, with the possible exception of the Aleutian Basin, were formed by back arc spreading as it is postulated for the Kurile Basin. In the Bowers, Komandorsky, Japan, and Aleutian basins, (possible) fossil spreading centers have been revealed based on basement features and/or magnetic anomalies. In the Kurile Basin, a N–S-striking rise has been identified that resembles a fossil spreading center.

The ages of the Aleutian and Bowers Basins are not clearly established. The Japan Basin opened in Early Miocene and the Komandorsky Basin was formed from 20 to 10 Ma in the rear of a dextral shear zone, which is the western segment of the Aleutian arc. Recently, displacements along this zone continue, which have led to the formation of pull-apart basins in the front and rear of the Komandorsky Islands. The Japan Sea also opened as a complex pull-apart basin along a dextral shear zone. Extension changed to compression at 12 Ma resulting in subsidence of the basin.

Our new data indicate that the opening of the Kurile basin began 26 My. ago with fairly slow spreading rates of 1.3–1.8 cm/y. The integration of these data with published data suggests that the processes of subduction, Kurile Basin opening and formation of the KFEZ occurred synchronously and that extension in the rear part and in the frontal part of the Kurile Island Arc are likely to have been triggered by the same mechanism. A shear zone could be a such mechanism and dextral displacements along this zone could have caused the opening of the Kurile Basin and the formation of the KFEZ, similar to the geodynamic situation that existed and still exists in the Komandorsky Basin.

**Supplementary Materials:** The following are available online at [www.mdpi.com/2076-3263/10/11/442/s1](http://www.mdpi.com/2076-3263/10/11/442/s1), Table S1: Measured and reference values for XRF standards, Table S2: Measured and reference values for ICP-MS standards BCR-2 (Univ. Bremen) and BIR-1 (Univ. Kiel).

**Author Contributions:** Conceptualization, R.W., B.B. and K.H.; methodology, R.W., B.B., P.v.d.B. and F.H.; validation, R.W., B.B., K.H., P.v.d.B., F.H. and I.T.; formal analysis, P.v.d.B. and F.H.; investigation, R.W., B.B., K.H., P.v.d.B., F.H. and I.T.; resources, R.W., B.B., P.v.d.B. and F.H.; data curation, R.W., B.B., P.v.d.B. and F.H.; writing—original draft preparation, R.W. and B.B.; writing—review and editing, R.W., B.B., K.H., P.v.d.B., F.H. and I.T.; visualization, R.W. and B.B.; supervision, B.B. and K.H.; project administration, R.W., B.B. and K.H.; funding acquisition, R.W., B.B. and K.H. All authors have read and agreed to the published version of the manuscript.

**Funding:** This research was funded by the German Ministry of Education and Research (BMBF), grant numbers 03G0568A (KOMEX II) and 03G0178A (SO178), and the Russian Ministry of Education and Science, grant number 2202. The processing of the bathymetric data carried out by B.B. was partially funded by state assignment of the Shirshov Institute of Oceanology Russian Academy of Sciences, theme No. 0149-2019-005.

**Acknowledgments:** We thank D. Rau, D. Garbe-Schönberg, A. Klügel, and S. Hauff for analytical and technical assistance. We are also grateful to R. Kulinich, chief scientist of RV Akademik Lavrentyev cruise 29, and W.-Chr. Dullo, chief scientist of R/V Sonne cruise SO178, the LV 29 and SO178 crews and shipboard scientific parties, and N. Biebow, K. Georgeleit and E.P. Lelikov for the support necessary to carry out this study. We further thank two anonymous reviewers for constructive reviews that helped improve this manuscript, as well as C. Chen and A. Zhang for editorial handling.

**Conflicts of Interest:** The authors declare no conflict of interest.

## References

1. Savostin, L.A.; Zonenshain, L.P.; Baranov, B.V. Geology and plate tectonics of the Sea of Okhotsk. In *Geodynamics of the Western Pacific*; Hilde, T.W.H., Uyeda, S., Eds.; AGU Geodynamics Series 11; AGU Publications: Washington, DC, USA, 1983; pp. 189–221.
2. Kimura, G.; Tamaki, K. Collision; rotation; and back-arc spreading in the region of the Okhotsk and Japan Seas. *Tectonics* **1986**, *5*, 386–401.
3. Jolivet, L. American-Eurasia plate boundary in eastern Asia and the opening of marginal seas. *Earth Planet. Sci. Lett.* **1987**, *81*, 282–288.
4. Maeda, J. Opening of the Kurile Basin deduced from the magmatic history of Central Hokkaido; North Japan. *Tectonophysics* **1990**, *174*, 235–255.
5. Gnibidenko, H.S.; Hilde, T.W.C.; Gretskeya, E.V.; Andreev, A.A. Kurile (South Okhotsk) back-arc basin. In *Back-Arc Basins: Tectonics and Magmatism*; Taylor, B., Ed.; Plenum: New York, NY, USA, 1995; pp. 421–449.
6. Baranov, B.; Wong, H.K.; Dozorova, K.; Kimura, B.; Lüdmann, T.; Karnaukh, V. Opening geometry of the Kurile Basin (Okhotsk Sea) as inferred from structural data. *Island Arc* **2002**, *11*, 206–219.
7. Kharakhin, V.V. Tectonics and development history of the sedimentary basins. In *Structure and Dynamics of the Lithosphere and Asthenosphere of the Okhotsk Region*; Rodnikov, A.G., Tuezov, I.K., Kharakhin, V.V., Eds.; Russian Academy of Sciences: Moscow, Russia, 1996; pp 256–305. (In Russian)
8. Hayashi, T. The Study of Thermal Structure and Tectonic History of the Derugin Basin; Sea of Okhotsk. Master's Thesis, Earthquake Research Institute, University of Tokyo, Tokyo, Japan, 1997.
9. Karp, B.Y.; Karnaukh, V.N.; Baranov, B.V.; Dozorova, K.A. Seismic stratigraphy and sedimentary processes on the Kurile Basin northern slope (Okhotsk Sea). *Mar. Geol.* **2006**, *228*, 1–14.
10. Terekhov, E.P.; Tsoy, I.B.; Vashchenkova, N.G.; Mozherovskii, A.V.; Gorovaya, M.T. Sedimentation Settings and Evolution History of the Kuril Basin (Sea of Okhotsk) in the Cenozoic. *Oceanology* **2008**, *48*, 609–617.
11. Emel'yanova, T.A.; Lelikov, E.P. Geochemistry and Petrogenesis of the Late Mesozoic–Early Cenozoic Volcanic rocks of the Okhotsk and Japan Marginal Seas. *Geochem. Int.* **2016**, *54*, 509–521.
12. Takeuchi, T.; Kodama, K.; Ozawa, T. Paleomagnetic evidence for block rotations in central Hokkaido-south Sakhalin, Northeast Asia. *Earth Planet. Sci. Lett.* **1999**, *169*, 7–21.
13. Ikeda, Y.; Stern, R.; Kagami, H.; Sun, C.-H. Pb, Nd, and Sr isotopic constraints on the origin of Miocene basaltic rocks from northeast Hokkaido, Japan: Implications for opening of the Kurile back-arc basin. *Island Arc* **2000**, *9*, 161–172.
14. Avdeiko, G.P.; Volynets, O.N.; Antonov, A.Y.; Bondarenko, V.I.; Rashidov, V.A.; Gladkov, N.G. Catalogue of submarine volcanoes of the Kurile Arc, North Iturup group. In *Submarine Volcanism and Zonality of the Kurile Island Arc*; Puscharovsky, Y.M., Ed.; Nauka: Moscow, Russia, 1992; pp. 172–198. (In Russian)
15. Lelikov, E.P.; Emel'yanova, T.A.; Baranov, B.V. Magmatism of the submarine Vityaz Ridge (Pacific slope of the Kurile Island Arc). *Oceanology* **2008**, *48*, 239–249.
16. Emel'yanova, T.A.; Lelikov, E.P.; Kostitsyn, Y.A. Geochemistry of the submarine Vityaz Ridge at the Pacific slope of the Kurile Island Arc. *Geochem. Int.* **2012**, *50*, 289–303.
17. Baranov, B.V.; Werner, R.; Hoernle, K.A.; Tsoy, I.B.; Bogaard, P.v.d.; Tararin, I.A. Evidence for compressionally induced high subsidence rates in the Kurile Basin (Okhotsk Sea). *Tectonophysics* **2002**, *350*, 63–97.
18. Tuezov, I.K. Submarine volcanoes of the Kurile Basin (Okhotsk Sea). *Pap. Acad. Sci. USSR* **1977**, *232*, 198–200. (In Russian).
19. Nürnberg, D.; Baranov, B.V.; Karp, B.Y. *R/V Akademik M. A. Lavrentyev Cruise 27*; GEOMAR Reports: Kiel, Germany, 1997; pp. 1–69.

20. Biebow, N.; Hütten, E. *Cruise Report KOMEX I and II: RV Professor Gagarinsky Cruise 22; RV Akademik M. A. Lavrentiev Cruise 28*; GEOMAR Reports: Kiel, Germany, 1999; pp. 1–188.
21. Galperin, E.I.; Kosminskaya, I.P. (Eds.) *Structure of the Earth's Crust in the Transition Zone from the Asian Continent to the Pacific Ocean*; Science: Moscow, Russia, 1964; pp. 1–306.
22. Biebow, N.; Kulinich, R.; Baranov, B. *KOMEX II, Kurile Okhotsk Sea Marine Experiment: Cruise Report RV Akademik M.A.Lavrentyev Cruise 29, Leg 1 and Leg 2*; IFM-GEOMAR: Kiel, Germany, 2003; p. 190.
23. Dullo, W.C.; Biebow, N.; Georgeleit, K. *SO178-KOMEX Cruise Report: Mass Exchange Processes and Balances in the Okhotsk Sea*; IFM-GEOMAR: Kiel, Germany, 2004; p. 125.
24. Lanphere, M.A.; Dalrymple, G.B. First-principles calibration of  $^{38}\text{Ar}$  tracers; implications for the ages of  $^{40}\text{Ar}/^{39}\text{Ar}$  fluence monitors. *USGS Prof. Pap.* **2000**, 1621, 1–10.
25. Garbe-Schönberg, C.-D. Simultaneous determination of thirty-seven trace elements in twenty-eight international rock standards by ICP-MS. *Geostand. Newsl.* **1993**, 17, 81–97.
26. Schwarz, S.; Klügel, A.; van den Bogaard, P.; Geldmacher, J. Internal structure and evolution of a volcanic rift system in the eastern North Atlantic: The Desertas rift zone, Madeira archipelago. *J. Volcanol. Geotherm. Res.* **2005**, 14, 123–155.
27. Hoernle, K.; Tilton, G. Sr-Nd-Pb isotope data for Fuerteventura (Canary Islands) basal complex and subaerial volcanics: Applications to magma genesis and evolution. *Schw. Mineral. Petrograph. Mitt.* **1991**, 71, 5–21.
28. Todt, W.; Cliff, R.A.; Hanser, A.; Hofmann, A.W.H. Evaluation of a  $^{202}\text{Pb}$ - $^{205}\text{Pb}$  double spike for high precision lead isotope analyses. In *Earth Processes: Reading the Isotopic Code*; Hart, S., Ed.; AGU: Washington, DC, USA, 1996; Volume 95, pp. 429–437.
29. Karp, B.Y.; Baranov, B.V.; Karnaukh, V.N.; Prokudin, V. Refraction seismics. In *Cruise Report R/V Akademik M.A.Lavrentiev Cruise 29; Leg 1 and 2*; Biebow, N., Kulinich, R., Baranov, B., Eds.; GEOMAR Reports: Kiel, Germany, 2003; pp. 176–184.
30. Werner, R.; Tararin, I.; Lelikov, E.P.; Baranov, B. Petrology and Volcanology. In *Cruise Report R/V Akademik M.A. Lavrentiev cruise 29; Leg 1 and 2*; Biebow, N., Kulinich, R., Baranov, B., Eds.; GEOMAR Reports: Kiel, Germany, 2003; pp. 168–174.
31. Werner, R.; Tararin, I.; Baranov, B. Petrology and Volcanology. In *SO178-KOMEX Cruise Report: Mass Exchange Processes and Balances in the Okhotsk Sea*; Dullo, W.C., Biebow, N., Georgeleit, K., Eds.; IFM-GEOMAR: Kiel, Germany, 2004; pp. 115–121.
32. Ludwig, K.R. *Isoplot 3.00: A Geochronological Toolkit for Microsoft Excel*; Special Publication No. 4; Berkeley Geochronological Center: Berkeley, CA, USA, 2003; pp. 1–74.
33. Le Bas, M.J.; Le Maitre, R.W.; Streckeisen, A.; Zanettin, B.A. Chemical classification of volcanic rocks based on the total alkali-silica diagram. *J. Petrol.* **1986**, 27, 745–750.
34. Hofmann, A.W. Chemical differentiation of the Earth: The relationship between mantle, continental crust, and oceanic crust. *Earth Planet. Sci. Lett.* **1988**, 90, 297–314.
35. McDonough, W.F.; Sun, S.-S. The composition of the Earth. *Chem. Geol.* **1995**, 120, 223–253.
36. Bindeman, I.N.; Bailey, J.C. Trace elements in anorthite megacrysts from the Kurile Island Arc: A window to across-arc geochemical variation in magma compositions. *Earth Planet. Sci. Lett.* **1999**, 169, 209–226.
37. Hoernle, K.; Werner, R.; Volynets, O.; Avdeiko, G.; Schmidt, A.; Wenskowski, B.; Doubik, P.; Tararin, I.A. Magma genesis beneath the Kurile Island arc: The fundamental role of fluids in subduction zones. In *Proceedings of the Third Workshop on Russian-German Cooperation in the Okhotsk Sea—Kurile Island arc system (KOMEX)*, Moscow, Russia, 17–19 April 2000; Institute of Oceanology: Moscow, Russia, 2000; p. 31.
38. Martynov, A.Y.; Kimura, J.-I.; Martynov, Y.A.; Rybin, A.V. Geochemistry of late Cenozoic lavas on Kunashir island, Kurile arc. *Island Arc* **2010**, 19, 86–104.
39. Martynov, Y.A.; Khanchuk, A.I.; Kimura, J.-I.; Rybin, A.V.; Martynov, A.Y. Geochemistry and petrogenesis of volcanic rocks in the Kurile island arc. *Petrology* **2010**, 18, 489–513.
40. Martynov, A.Y.; Martynov, Y.A.; Rybin, A.V.; Kimura, J.-I. Role of back-arc tectonics in the origin of subduction magmas: New Sr, Nd, and Pb isotope data from middle Miocene lavas of Kunashir island (Kurile island arc). *Russ. Geol. Geophys.* **2015**, 56, 363–378.
41. Martynova, A.Y. Role of backarc processes in the origin of across-arc geochemical zoning in volcanics of early evolutionary stages in Kunashir island. *Petrology* **2013**, 21, 471–488.

42. Martynov, A.Y.; Martynov, Y.A. Pleistocene basaltic volcanism of Kunashir island (Kurile island arc): Mineralogy, geochemistry, and results of computer simulation. *Petrology* **2017**, *25*, 206–225.
43. Zindler, A.; Hart, S.R. Chemical geodynamics. *Ann. Rev. Earth Planet. Sci.* **1986**, *14*, 493–571.
44. Hart, S.R.; Hauri, E.H.; Oschmann, L.A.; Whitehead, J.A. Mantle plumes and entrainment: Isotopic evidence. *Science* **1992**, *256*, 517–520.
45. Harvey, J.; Gannoun, A.; Burton, K.W.; Rogers, N.W.; Alard, O.; Parkinson, I.J. Ancient melt extraction from the oceanic upper mantle revealed by Re-Os isotopes in abyssal peridotites from the Mid-Atlantic ridge. *Earth Planet. Sci. Lett.* **2006**, *244*, 606–621.
46. Sergeev, K.P. *Tectonics of the Kurile Island System*; Science Publ.: Moscow, Russia, 1976; pp. 1–238. (In Russian)
47. Zlobin, T.K. *Crustal and Upper Mantle Structure of the Kurile Island Arc According to Seismic Data*; Far East Scientific Centre Publ.: Vladivostok, Russia, 1987; pp. 1–150. (In Russian)
48. Zonenshain, L.P.; Kuzmin, M.I.; Natapov, L.M. *Plate Tectonics of the USSR Territory*; Nedra Publ.: Moscow, Russia, 1990; pp. 1–332. (In Russian)
49. Verzhbitsky, E.V.; Kononov, M.V. *Lithosphere Genesis of the Northern World Ocean*; Scientific World Publ.: Moscow, Russia, 2010; pp. 1–477. (In Russian)
50. Laverov, N.P.; Lappo, S.S.; Lobkovsky, L.I.; Baranov, B.V.; Kulinich, R.G.; Karp, B.Y. Central Kurile gap: Structure and seismic potential. *Dokl. Earth Sci.* **2006**, *409*, 787–790.
51. Kulinich, R.G.; Karp, B.Y.; Baranov, B.V.; Lelikov, E.P.; Karnaukh, V.N.; Valitov, M.G.; Nikolaev, S.M.; Kolpashchnikova, T.N.; Tsoi, I.B. Structural and Geological Characteristics of a “Seismic Gap” in the Central Part of the Kuril Island Arc. *Russ. J. Pac. Geol.* **2007**, *1*, 3–14.
52. Baranov, B.V.; Seliverstov, N.I.; Murav'ev, A.V.; Muzurov, E.L. The Komandorsky basin as a product of spreading behind a transform plate boundary. *Tectonophysics* **1991**, *199*, 237–270.
53. Kimura, G. Oblique subduction and collision, Forearc tectonics of the Kuril arc. *Geology* **1986**, *14*, 404–407.
54. Tu Zino, T.; Murakami, F. Evolution of collision-related basins in the eastern end of the Kurile Basin; Okhotsk Sea. NW. *Pac. J. Asian Earth Sci.* **2008**, *33*, 1–24.
55. Fournier, M.; Jolivet, L.; Huchson, P.H.; Sergeev, K.F.; Ocorbin, L.S. Neogene strike-slip faulting in Sakhalin and Japan Sea. *J. Geophys. Res.* **1994**, *99*, 2701–2725.
56. Cormier, V.F. Tectonics near the junction of the Aleutian and Kuril–Kamchatka area and a mechanism for the middle Tertiary magmatism in the Kamchatka Basin. *Geol. Soc. Am. Bull.* **1975**, *86*, 443–453.
57. Seliverstov, N.I. *Sea Bottom Structure off Kamchatka and Geodynamics of the Kamchatka/Aleutian Junction Area*; Science: Moscow, Russia, 1998. (In Russian)
58. Barth, G.A.; Scheirer, D.S.; Christeson, G.L.; Stern, R.J.; Scholl, D.W. New geophysical constraints on the tectonic history of the Bering Sea. In Proceedings of the AGU Fall Meeting, San Francisco, CA, USA, 3–7 December 2012; AGU: Washington, DC, USA, 2012; T51D-2625.
59. Cooper, A.K.; Marlow, M.S.; Scholl, D.W. Bering Sea—A multifarious marginal basin. In *Island Arcs, Deep Sea Trenches and Back-Arc Basins*; Talwani, M., Pitman, W.C., III, Eds.; AGU Maurice Ewing Series; AGU: Washington, DC, USA, 1977; Volume 1, pp. 437–450.
60. Cooper, A.K.; Marlow, M.S.; Scholl, D.W.; Stevenson, A.J. Evidence for Cenozoic crustal extension in the Bering Sea region. *Tectonics* **1992**, *11*, 719–731.
61. Scheirer, D.S.; Barth, G.A.; Scholl, D.W.; Stern, R.J. New Magnetic Anomaly Compilation Illuminates the Formation of the Aleutian Basin. In Proceedings of the AGU Fall Meeting, San Francisco, CA, USA, 9–13 December 2013; AGU: Washington, DC, USA, 2013; OS13B-1706.
62. Scholl, D.W.; Buffington, E.C.; Marlow, M.S. Plate tectonics and the structural evolution of the Aleutian-Bering Sea region. In *Contribution to the Geology of the Bering Sea Basin and Adjacent Regions*; Forbes, R.R., Ed.; Geological Society of America Special Paper: Boulder, CO, USA, 1975; Volume 15, pp. 1–31.
63. Sharp, W.D.; Clague, D.A. 50-Ma Initiation of Hawaiian-Emperor Bend Records Major Change in Pacific Plate Motion. *Science* **2006**, *313*, 1281–1284.
64. Jicha, B.R.; Scholl, D.W.; Singer, B.S.; Yogodzinski, G.M.; Kay, S.M. Revised age of Aleutian Island Arc formation implies high rate of magma production. *Geology* **2006**, *34*, 661–664.
65. Stern, R.J.; Barth, G.A.; Scheirer, D.S.; Scholl, D.W. Did the Bering Sea Form as a Cenozoic Backarc Basin? In Proceedings of the AGU Fall Meeting, San Francisco, CA, USA, 3–7 December 2012; AGU: Washington, DC, USA, 2012; T54A-06.

66. Xu, J.; Ben-Avraham, Z.; Kelty, T.; Yu, H.-S. Origin of marginal basins of the NW Pacific and their plate tectonic reconstructions. *Earth Sci. Rev.* **2014**, *130*, 154–196.
67. Scholl, D.W. Viewing the tectonic evolution of the Kamchatka-Aleutian (KAT) connection with an Alaska crustal extrusive perspective. In *Volcanism and Subduction: The Kamchatka Region*; Eichelberger, J., Gordeev, E., Izbekov, P., Kasahara, M., Lees, J., Eds.; AGU Geophysical Monograph: Washington, DC, USA, 2007; Volume 172, pp. 3–36.
68. Wanke, M.; Portnyagin, M.; Hoernle, K.; Werner, R.; Hauff, F.; van den Bogaard, P.; Garbe-Schönberg, D. Bowers Ridge (Bering Sea): An Oligocene–Early Miocene island arc. *Geology* **2012**, *40*, 687–690.
69. Cooper, A.K.; Marlow, M.S.; Ben-Avraham, Z.V.I. Multichannel seismic evidence bearing on the origin of Bowers Ridge, Bering Sea. *Geol. Soc. Am. Bull.* **1981**, *92*, 474–484.
70. Redfield, T.F.; Scholl, D.W.; Fitzgerald, P.G.; Beck, M.E. Escape tectonics and the extrusion of Alaska: Past, present, and future. *Geology* **2007**, *35*, 1039–1042.
71. Valyashko, G.M.; Chernyavsky, G.B.; Seliverstov, N.I.; Ivanenko, A.N. Backarc spreading in the Komandorsky Basin. *Pap. Acad. Sci. USSR* **1993**, *338*, 212–216. (In Russian)
72. Geist, E.L.; Scholl, D.W. Large-scale deformation related to the collision of the Aleutian Arc with Kamchatka. *Tectonics* **1994**, *13*, 536–560.
73. Gaedicke, C.H.; Baranov, B.; Seliverstov, N.; Alexeiev, D.; Tsukanov, N.; Freitag, R. Structure of an active arc–continent collision area: The Aleutian–Kamchatka junction. *Tectonophysics* **2000**, *325*, 63–85.
74. Tamaki, K. Geological structure of the Japan Sea and its tectonic implications. *Bull. Geol. Surv. Jpn.* **1988**, *39*, 269–365.
75. Tamaki, K.; Pisciotto, K.; Allan, J. *Initial Reports ODP Leg 127 Japan Sea*; Ocean drilling Program: College Station, TX, USA, 1990, Volume 127, doi:10.2973/odp.proc.ir.127.1990.
76. Jolivet, L.; Tamaki, K. Neogene kinematics in the Japan Sea Region and volcanic activity of the Northeast Japan Arc. In *Proceedings of the Ocean Drilling Program, Scientific Results*; Tamaki, K., Suyehiro, K., Allan, J., McWilliams, M., Eds.; Ocean drilling Program: College Station, TX, USA, 1992; Volume 127/128, Part 2, pp. 1311–1331, doi:10.2973/odp.proc.sr.127128-2.132.1992.
77. Ingle, J.C., Jr. Subsidence of the Japan Sea: Stratigraphic evidence from ODP sites and onshore sections. In *Proceedings of the Ocean Drilling Program, Scientific Results*; Tamaki, K., Suyehiro, K., Allan, J., McWilliams, M., Eds.; Ocean drilling Program: College Station, TX, USA, 1992; Volume 127/128, Part 2, pp. 1197–1218, doi:10.2973/odp.proc.sr.127128-2.132.1992.

**Publisher’s Note:** MDPI stays neutral with regard to jurisdictional claims in published maps and institutional affiliations.



© 2020 by the authors. Licensee MDPI, Basel, Switzerland. This article is an open access article distributed under the terms and conditions of the Creative Commons Attribution (CC BY) license (<http://creativecommons.org/licenses/by/4.0/>).